RESEARCH ARTICLE

Persymmetric Two-Step-Based Detectors for Range-Spread Targets against Compound-Gaussian Clutter

Tao Jian[1,2,*], Zikeng Xie[1,2], Jia He[1,2], Lei Guo[3] and Xiaoming Tang[4]

[1] Research Institute of Information Fusion, Naval Aviation University, Yantai 264001, China
[2] Key Laboratory of Sea-Air Information Perception and Processing Technology of Shandong Provincial, Yantai 264001, China
[3] Unit 92830 of PLA, Haikou 570100, China
[4] The 3H Company, Yantai 264001, China

Abstract

This research addresses the challenge of detecting radar range-spread targets in compound-Gaussian clutter environments. In such scenarios, the target signals occupy unknown coordinates within a subspace, while the clutter is modeled as compound-Gaussian distribution involving inverse Gamma textures and complex Gaussian speckles with an unknown persymmetric covariance matrix. Additionally, we assume the availability of training data for estimating clutter covariance matrix. Utilizing a two-step approach, three detectors are proposed according to the Gradient, Rao, and Wald tests, by taking advantage of the persymmetry of the clutter covariance matrix. Theoretical analyses demonstrate that the proposed detectors maintain an asymptotically constant false alarm rate relative to the structure of the clutter covariance matrix. Furthermore, Monte Carlo simulations have yielded numerical evidence indicating that the proposed detectors outperform the current contrastive approaches, especially in cases where the training data is scarce.

Keywords: compound-Gaussian clutter, range-spread targets, persymmetry, gradient test, rao test, wald test.

1 Introduction

In scenarios involving high-resolution radar (HRR) detection, the scattered energy from target generally disperses across several neighboring range cells, leading to the creation of range-spread targets [1–3]. Currently, numerous detectors for detecting range-spread targets have been primarily designed and been further optimized for operation in homogeneous environments (HE) [4–6], where it is assumed that the clutter components in the range cell under test have the same covariance matrix as the training data consisting of clutter only. However, in detection

Academic Editor:
Hongqi Fan

Submitted: 27 June 2025
Accepted: 03 September 2025
Published: 03 November 2025

Vol. 2, **No.** 4, 2024.
10.62762/CJIF.2025.664545

***Corresponding author:**
Tao Jian
work_jt@163.com

Citation
Jian, T., Xie, Z., He, J., Guo, L., & Tang, X. (2025). Persymmetric Two-Step-Based Detectors for Range-Spread Targets against Compound-Gaussian Clutter. *Chinese Journal of Information Fusion*, 2(4), 296–312.

modes characterized by low grazing angles or HRR, the clutter exhibits increasingly strong non-Gaussian characteristics [7], making the detectors designed for HE difficult to apply.

As one of the typical non-Gaussian models, the compound-Gaussian distribution is extensively employed to characterize the non-Gaussian statistical attributes of the actual clutter [8]. Preliminary researches have been conducted on the adaptive detection of range-spread targets within compound-Gaussian clutter. For example, three detectors are designed for the point targets and the range-spread targets in [9] and [10] respectively, by utilizing the one-step generalized likelihood ratio test (GLRT), the maximum a posteriori (MAP) GLRT, and the two-step GLRT. In [11] the adaptive detection approaches are investigated for range-spread targets, employing the two-step Rao and Wald test criteria. It is worth noting that the aforementioned adaptive detectors [9, 10, 12–14] are all based on the rank-one signal model and assume that the target steering vector is already known.

Nonetheless, in real-world scenarios, due to the influence of factors such as beam pointing errors and multipath effects [15–19], it is sometimes challenging to obtain accurate target steering vectors. To address this issue, it might be reasonable to consider modeling the target signal as a subspace signal [20], more precisely, we assume the target signal lies within a known multi-rank subspace, with its specific coordinates remaining unknown. The subspace model has already demonstrated its effectiveness in numerous methods [21–23]. For example, by utilizing a two-step design process, the subspace models are employed in [24] to explore radar detectors for range-spread targets within compound-Gaussian clutter. Different detection frameworks are developed by applying the GLRT, Wald, Gradient, Rao, and Durbin tests (labeled as S-GLRT-CG, S-Wald-CG, S-Rao-CG, S-Gradient-CG and S-Durbin-CG). For this case, identical results are demonstrated for the detection mechanisms based on the Gradient, Rao, and Durbin tests. It is noteworthy that the clutter texture components are modeled as the deterministic unknowns, which are subsequently solved by employing the maximum likelihood (ML) estimation. However, owing to the oversight of potential prior distribution related to the clutter texture components, the efficacy of the introduced detectors might be compromised under certain texture configurations within the compound-Gaussian clutter. Recently, as the research about compound-Gaussian models has intensified, the modeling of clutter texture components has become increasingly refined. Existing research results indicate that the clutter texture components fit well the inverse Gamma distribution [25]. Within the realm of compound-Gaussian clutter, the absence of a uniformly most powerful invariant test for range-spread target detection necessitates further exploration of adaptive detectors that rely on diverse testing criteria. In addition, it is known that target-free training data should be at least twice the channel cardinality to achieve desirable detection performance [26, 27]; otherwise, the detector will suffer a relatively large performance penalty. However, the available training data are always insufficient in numerous real-world situations, including those with pronounced multipath effects, outliers, and irregular topographical features [28–32]. Considering the radar receiver employing symmetrically structure for spatial processing (arrays) or temporal processing (coherent pluses) [33–35], the clutter covariance matrix (CCM) possesses the persymmetric structure which can be used to potentially reduce the training data requirement for detector design. With the persymmetry leveraged, detecting a rank-one point-like target is considered within compound-Gaussian clutter [36], assuming the texture follows either a Gamma distribution or an inverse Gamma distribution, and the two-step GLRT is employed for this purpose. Meanwhile, the two-step Rao and two-step Wald tests are devised in [37] to detect a rank-one range-spread target in compound-Gaussian clutter, specifically assuming that the texture conforms to an inverse Gamma distribution (denoted as P-Rao-iGCG and P-Wald-iGCG).

Drawing inspiration from the previously cited works, we harness the persymmetry property of the CCM to design three detectors tailored for identifying range-spread targets within compound-Gaussian clutter characterized by an inverse Gamma texture. The primary contributions of this paper are summarized below:

1. By employing a two-step approach, we develop three detection schemes based on the Gradient, Rao, and Wald tests for detecting range-spread targets in compound-Gaussian clutter with inverse Gamma texture. Interestingly, the Gradient-based and Rao-based detectors are theoretically demonstrated to be equivalent.

2. All of these developed persymmetric detectors are proved to provide an asymptotically constant false alarm rate (CFAR) in relation to the structure of the CCM, as demonstrated both theoretically and through simulations.

3. Numerical results demonstrate that the developed detectors outperform their competitors under both matched and mismatched conditions, across different training data sizes, with particularly notable advantages in scenarios where training data is limited.

The structure of this paper is outlined as follows: Section 2 offers a comprehensive introduction to the problem under investigation. Section 3 details the derivation of detectors based on a two-step design procedure. Section 4 showcases the numerical findings, while the concluding remarks are encapsulated in Section 5.

Notations

The superscripts $(\cdot)^*$, $(\cdot)^T$ and $(\cdot)^H$ represent the conjugate, the transpose and the conjugate transpose, respectively. $\mathbf{I}_m$ represents an $m \times m$ unit matrix, $\mathbf{0}_{m\times n}$ signifies an $m \times n$ zero matrix, and $j = \sqrt{-1}$ stands for the imaginary unit. $\mathbf{C}^{m\times n}$ refers to an $m \times n$ Euclidean space composed of complex matrices. $\mathrm{tr}(\cdot)$ indicates the trace of a square matrix. $\mathrm{vec}(\cdot)$ represents the conversion of a matrix into a vector. $\mathbf{CN}(x, \Sigma_1)$ denotes the circular complex Gaussian distribution with mean-vector x and covariance matrix Σ_1, while $\mathbf{CW}(n, \Sigma_2)$ indicates the complex central Wishart distribution with n degrees of freedom and a given scale matrix Σ_2. $\mathbf{P}_A$ signifies the orthogonal projection matrix onto the subspace spanned by the columns of matrix $\mathbf{A}$, specifically calculated as $\mathbf{P}_A = \mathbf{A}(\mathbf{A}^H\mathbf{A})^{-1}\mathbf{A}^H$. $\ln(\cdot)$ represents the natural logarithm of a scalar-valued function, and $\partial g/\partial \mathbf{\Psi}$ is the partial derivative of g with respect to (w.r.t) $\mathbf{\Psi}$, where $\mathbf{\Psi}$ is a vector or matrix. $\Re e$ and $\Im m$ represent the real part and the imaginary part, respectively.

2 Problem formulation

Imagine a scenario where a target is dispersed over K range cells. The vector $\mathbf{z}_k \in \mathbf{C}^{N\times 1}$, $k = 1, 2, \cdots, K$ represents the test data gathered from the kth range cell under test (CUT), with N indicating the joint space-time dimension. The echo signal from the target in the kth range cell can be represented as a subspace vector $\mathbf{s}_k = \mathbf{U}\mathbf{b}_k \in \mathbf{C}^{N\times 1}$, $k = 1, 2, \cdots, K$, where the subspace matrix $\mathbf{U} \in \mathbf{C}^{N\times r}$ is a known full-column-rank matrix with rank r, and the vector $\mathbf{b}_k \in \mathbf{C}^{r\times 1}$ denotes an unknown complex coordinate vector. Furthermore, the clutter components $\mathbf{c}_k \in \mathbf{C}^{N\times 1}$, $k = 1, 2, \cdots, K$ in the CUT are presumed to be independent and identically distributed (IID). More precisely, it exhibits a compound-Gaussian distribution, which can be characterized as $\mathbf{c}_k = \sqrt{\tau_k} g_k$. Herein, the variable τ_k, $k = 1, 2, \cdots, K$, denoted as a positive random variable, is commonly known as texture and signifies the local power of clutter. Meanwhile, the speckle $\mathbf{g}_k$, an N-dimensional random vector, is typically identified as a Gaussian distribution and captures the clutter characteristics of the joint space-time domain.

Regarding the distribution of the texture component τ_k, we examine the situation where it follows an inverse-Gamma distribution [9, 10, 25]. In such a case, the probability density function (PDF) of τ_k can be expressed as follows:

$$f(\tau_k) = \frac{\beta_k^{q_k}}{\Gamma(q_k)\tau_k^{q_k+1}} \exp\left(-\frac{\beta_k}{\tau_k}\right), \tau_k \geq 0, q_k \geq 0, \beta_k \geq 0 \tag{1}$$

where q_k and β_k are shape and scale parameters, respectively; the speckle component $\mathbf{g}_k$ is characterized as a Gaussian vector with zero mean and unknown CCM $\mathbf{M}$, i.e., $g_k \sim \mathbf{CN}(\mathbf{0}_{N\times 1}, \mathbf{M})$. Consequently, under the hypothesis H_0, which assumes the absence of target signal and the presence of clutter only, the expression for $\mathbf{z}_k$ can be formulated as follows:

$$\mathbf{z}_k = \mathbf{c}_k, \quad k = 1, 2, \cdots, K \tag{2}$$

Meanwhile, under the alternative hypothesis H_1, which assumes the presence of target signal, the vector $\mathbf{z}_k$ can be represented as:

$$\mathbf{z}_k = Ub_k + \mathbf{c}_k, \quad k = 1, 2, \cdots, K \tag{3}$$

Additionally, for the estimation of the unknown CCM $\mathbf{M}$, it is usually assumed that a collection of training data from R cells neighboring the CUT, devoid of target signal echoes, is available [38]. The training data can be formulated as $\mathbf{y}_l = \mathbf{c}_l, \quad l = 1, 2, \cdots, R$, with $\mathbf{c}_l \in \mathbf{C}^{N\times 1}$ being IID as the clutter components $\mathbf{c}_k$ in the CUT.

In summary, the framework for range-spread target detection can be expressed through a binary hypothesis test as follows:

$$
\begin{cases}
H_0: & \begin{cases} \mathbf{z}_k = \mathbf{c}_k, & k = 1, 2, \cdots, K \\ \mathbf{y}_l = \mathbf{c}_l, & l = 1, 2, \cdots, R \end{cases} \\
H_1: & \begin{cases} \mathbf{z}_k = \mathbf{U}\mathbf{b}_k + \mathbf{c}_k, & k = 1, 2, \cdots, K \\ \mathbf{y}_l = \mathbf{c}_l, & l = 1, 2, \cdots, R \end{cases}
\end{cases} \tag{4}
$$

3 Design of adaptive detectors

In this section, we are dedicated to developing three detectors specifically designed to solve the detection problem outlined in (4). These detectors are developed following a two-step design procedure, based on the principles of Rao, Wald, and Gradient tests. Additionally, this endeavor involves incorporating the concept of persymmetry into the design stage of these detectors, with the aim of enhancing their detection performance beyond that of existing detectors.

3.1 Data transformation

For radar systems utilizing symmetrical configurations in spatial processing (arrays) or temporal processing (coherent pulses) [39], the CCM $\mathbf{M}$ is observed to satisfy the condition $\mathbf{M} = \mathbf{D}_N \mathbf{M}^* \mathbf{D}_N$, with the $N \times N$ anti-diagonal matrix $\mathbf{D}_N$ being represented as:

$$
\mathbf{D}_N = \begin{bmatrix} 0 & 0 & \cdots & 0 & 1 \\ 0 & 0 & \cdots & 1 & 0 \\ \vdots & \vdots & \ddots & \vdots & \vdots \\ 0 & 1 & \cdots & 0 & 0 \\ 1 & 0 & \cdots & 0 & 0 \end{bmatrix}_{N \times N} \tag{5}
$$

Moreover, each column within the subspace matrix $\mathbf{U}$ is also expected to exhibit the persymmetry, meaning $\mathbf{U} = \mathbf{D}_N \mathbf{U}^*$. By leveraging the persymmetry of the CCM, we can obtain:

$$
\begin{aligned}
&\mathrm{tr}\left(\mathbf{M}^{-1} (\mathbf{z}_k - i\mathbf{U}\mathbf{b}_k)(\mathbf{z}_k - i\mathbf{U}\mathbf{b}_k)^H\right) \\
&\quad = \mathrm{tr}\left(\mathbf{M}^{-1} (\mathbf{z}_{pk} - i\mathbf{U}\mathbf{b}_{pk})(\mathbf{z}_{pk} - i\mathbf{U}\mathbf{b}_{pk})^H\right), \\
&\quad i = 0, 1; \quad k = 1, 2, \cdots, K
\end{aligned} \tag{6}
$$

where

$$
\begin{cases} \mathbf{z}_{pk} = [\mathbf{z}_{ek}, \mathbf{z}_{ok}] \in \mathbf{C}^{N \times 2} \\ \mathbf{b}_{pk} = [\Re e(\mathbf{b}_k), j\Im m(\mathbf{b}_k)] \in \mathbf{C}^{r \times 2} \end{cases} \tag{7}
$$

with

$$
\begin{cases} z_{ek} = \frac{1}{2}(\mathbf{z}_k + \mathbf{D}_N \mathbf{z}_k^*) \in \mathbf{C}^{N \times 1} \\ z_{ok} = \frac{1}{2}(\mathbf{z}_k - \mathbf{D}_N \mathbf{z}_k^*) \in \mathbf{C}^{N \times 1} \end{cases} \tag{8}
$$

Consequently, the conditional PDF of $\mathbf{Z}_p = [\mathbf{z}_{p1}, \mathbf{z}_{p2}, \cdots, \mathbf{z}_{pK}] \in \mathbf{C}^{N \times 2K}$ can be expressed as

$$
\begin{aligned}
f_i(\mathbf{Z}_p|\boldsymbol{\Theta}) = \prod_{k=1}^{K} \frac{1}{\pi^N |\mathbf{M}| \tau_k^N} \exp\left\{ -\frac{\mathrm{tr}\left[\mathbf{M}^{-1}(\mathbf{z}_{pk} - i\mathbf{U}\mathbf{b}_{pk})(\mathbf{z}_{pk} - i\mathbf{U}\mathbf{b}_{pk})^H\right]}{\tau_k} \right\}, \\
i = 0, 1
\end{aligned} \tag{9}
$$

where $\boldsymbol{\Theta} = \left[\boldsymbol{\Theta}_t^T, \boldsymbol{\Theta}_s^T\right]^T \in \mathbf{C}^{(2r+1)KN}$, with $\boldsymbol{\Theta}_t = \mathrm{vec}([b_{p1}, b_{p2}, \cdots, b_{pK}]) \in \mathbf{C}^{2rKN}$ and $\boldsymbol{\Theta}_s = [\tau_1, \tau_2, \cdots, \tau_K]^T \in \mathbf{C}^{K \times 1}$.

3.2 Detector design for known M

In this subsection, we employ a two-step approach by utilizing the Rao, Wald, and Gradient tests to construct detectors. More specifically, we initially assume that the texture components $\tau_k, k = 1, 2, \cdots, K$ and the covariance matrix structure $\mathbf{M}$ are known. Under this premise, we derive the test statistics for three detectors. Following this, we incorporate the MAP estimate of τ_k and the fixed-point (FP) estimate of $\mathbf{M}$ into the previously derived test statistics, which allows us to develop fully adaptive decision-making frameworks.

3.2.1 Gradient test for known M

The detection statistics of Gradient test for the detection problem indicated in (4) can be expressed as [40]:

$$
\lambda_{\text{Gradient}} = \left.\frac{\partial \ln f_1(\mathbf{Z}_p|\boldsymbol{\theta})}{\partial \boldsymbol{\theta}^T}\right|_{\boldsymbol{\theta}=\hat{\boldsymbol{\theta}}_0}^{T} \left(\hat{\boldsymbol{\theta}}_{r1} - \boldsymbol{\theta}_{r0}\right) \tag{10}
$$

where $\hat{\boldsymbol{\theta}}_0$ represents the maximum likelihood (ML) estimate of $\boldsymbol{\theta}$ under H_0, $\hat{\boldsymbol{\theta}}_{r1}$ denotes the ML estimate of $\boldsymbol{\theta}_r$ under H_1, and $\boldsymbol{\theta}_{r0} = 0_{2rK \times 1}$ corresponds to the actual value of $\boldsymbol{\theta}_r$ under H_0.

By computing the partial derivative of (9) w.r.t $\boldsymbol{\Theta}_r$ under H_1, we can obtain

$$
\frac{\partial \ln f_1(\mathbf{Z}_p|\boldsymbol{\Theta})}{\partial \boldsymbol{\Theta}_r} = 2 \begin{bmatrix} \frac{\left\{(\mathbf{z}_{p1} - \mathbf{U}\,\mathbf{b}_{p1})^H \mathbf{M}^{-1}\mathbf{U}\right\}^T}{\tau_1}, & \frac{\left\{(\mathbf{z}_{p2} - \mathbf{U}\,\mathbf{b}_{p2})^H \mathbf{M}^{-1}\mathbf{U}\right\}^T}{\tau_2}, \\ & \cdots, \\ \frac{\left\{\left(\mathbf{z}_{pK} - \mathbf{U}\,\mathbf{b}_{pK}\right)^H \mathbf{M}^{-1}\mathbf{U}\right\}^T}{\tau_K} & \end{bmatrix}^T \tag{11}
$$

Due to the absence of target under H_0, we have $\mathbf{b}_{pk} = \mathbf{0}_{r \times 2}$, and then (11) can be rewritten as

$$
\left.\frac{\partial \ln f_0(\mathbf{Z}_p|\boldsymbol{\Theta})}{\partial \boldsymbol{\Theta}_r}\right|_{\boldsymbol{\theta}=\hat{\boldsymbol{\theta}}_0} = 2 \begin{bmatrix} \frac{\left\{z_{p1}^H M^{-1} U\right\}^T}{\tau_{1,0}}, & \frac{\left\{z_{p2}^H M^{-1} U\right\}^T}{\tau_{2,0}}, \\ & \cdots, \\ \frac{\left\{z_{pK}^H M^{-1} U\right\}^T}{\tau_{K,0}} & \end{bmatrix}^T \tag{12}
$$

where $\tau_{k,0}, k = 1, 2, \cdots, K$ represents the estimated value of τ_k under H_0.

By taking the derivative of $f_1(\mathbf{Z}_p|\boldsymbol{\Theta})$ in (9) w.r.t the unknown coordinate vector $\mathbf{b}_{pk}$ and then equating the derivative to zero, we can obtain the ML estimate of $\mathbf{b}_{pk}$ under H_1:

$$\hat{\mathbf{b}}_{pk} = \left(\mathbf{U}^H\mathbf{M}^{-1}\mathbf{U}\right)^{-1}\mathbf{U}^H\mathbf{M}^{-1}\mathbf{z}_{pk} \tag{13}$$

Substituting $\hat{\mathbf{b}}_{pk}$ into $\boldsymbol{\Theta}_r$, we can obtain the ML estimate of $\boldsymbol{\Theta}_r$ under H_1:

$$\begin{aligned}\hat{\boldsymbol{\Theta}}_{r1} = \mathrm{vec}\Big[&\left(\mathbf{U}^H\mathbf{M}^{-1}\mathbf{U}\right)^{-1}\mathbf{U}^H\mathbf{M}^{-1}\mathbf{z}_{p1},\\ &\left(\mathbf{U}^H\mathbf{M}^{-1}\mathbf{U}\right)^{-1}\mathbf{U}^H\mathbf{M}^{-1}\mathbf{z}_{p2},\\ &\cdots, \left(\mathbf{U}^H\mathbf{M}^{-1}\mathbf{U}\right)^{-1}\mathbf{U}^H\mathbf{M}^{-1}\mathbf{z}_{pK}\Big]\end{aligned} \tag{14}$$

Given the high computational complexity of the ML estimate of τ_k under H_0, subsequent steps will involve performing the MAP estimate of τ_k under H_0. From (1) and (9), the maximum a posteriori probability density function (MAP PDF) of τ_k under H_0 can be expressed as

$$f_0\left(\tau_k|\mathbf{Z}_p\right) = \frac{f_0\left(\mathbf{Z}_p|\boldsymbol{\Theta}\right) f\left(\tau_k\right)}{f_0\left(\mathbf{Z}_p\right)} \tag{15}$$

where $f_0(Z_p) = \int f_0(\mathbf{Z}_p|\boldsymbol{\Theta}) f(\tau_1) f(\tau_2)\cdots f(\tau_K) d\boldsymbol{\Theta}_s$ denotes the PDF of $\mathbf{Z}_p$ under H_0.

By differentiating $f_0(\tau_k|\mathbf{Z}_p)$ w.r.t τ_k and setting the derivative to zero, the MAP estimate of τ_k under H_0 can be obtained as

$$\hat{\tau}_{k,0} = \arg\max_{\tau_k} f_0(\mathbf{Z}_p|\boldsymbol{\Theta}) f(\tau_k) = \frac{\mathrm{tr}(\mathbf{z}_{pk}^H\mathbf{M}^{-1}z_{pk}) + \beta_k}{N + q_k + 1} \tag{16}$$

By substituting (12), (14), and (16) into (10) and simplifying the result, we can obtain the Gradient test statistics for given $\mathbf{M}$ as

$$\lambda_{\text{Gradient}} = \sum_{k=1}^{K}\frac{(N + q_k + 1)\,\mathrm{tr}(\mathbf{z}_{pk}^H\mathbf{P}_U\mathbf{z}_{pk})}{\mathrm{tr}(\mathbf{z}_{pk}^H\mathbf{M}^{-1}\mathbf{z}_{pk}) + \beta_k} \tag{17}$$

where $\mathbf{P}_U = \mathbf{M}^{-1}\mathbf{U}(\mathbf{U}^H\mathbf{M}^{-1}\mathbf{U})^{-1}\mathbf{U}^H\mathbf{M}^{-1}$.

3.2.2 *Rao test for known M*

The detection statistic based on the two-step Rao criterion for the detection problem indicated in (4) can be expressed as [41]

$$\lambda_{\text{Rao}} = \left.\frac{\partial \ln f_1(\mathbf{Z}_p|\boldsymbol{\Theta})}{\partial \boldsymbol{\Theta}_r}\right|_{\boldsymbol{\Theta}=\hat{\boldsymbol{\Theta}}_0}^T \left[\mathbf{I}^{-1}(\hat{\boldsymbol{\Theta}}_0)\right]_{\boldsymbol{\Theta}_r,\boldsymbol{\Theta}_r} \left.\frac{\partial \ln f_1(\mathbf{Z}_p|\boldsymbol{\Theta})}{\partial \boldsymbol{\Theta}_r^*}\right|_{\boldsymbol{\Theta}=\hat{\boldsymbol{\Theta}}_0} \tag{18}$$

where the submatrix $\left[\mathbf{I}^{-1}(\boldsymbol{\Theta})\right]_{\boldsymbol{\Theta}_r,\boldsymbol{\Theta}_r}$ represents the portion of $\mathbf{I}^{-1}(\boldsymbol{\Theta})$ corresponding to the vector $\boldsymbol{\Theta}_r$, with $\mathbf{I}(\boldsymbol{\Theta})$ implying the Fisher Information Matrix w.r.t $\boldsymbol{\Theta}$, i.e.,

$$\mathbf{I}(\boldsymbol{\Theta}) = E\left\{\frac{\partial \ln f_1(\mathbf{Z}_p|\boldsymbol{\Theta})}{\partial \boldsymbol{\Theta}^*}\frac{\partial \ln f_1(\mathbf{Z}_p|\boldsymbol{\Theta})}{\partial \boldsymbol{\Theta}^T}\right\} \tag{19}$$

and according to the relevant components of $\boldsymbol{\Theta}_r$ and $\boldsymbol{\Theta}_s$, $\mathbf{I}(\boldsymbol{\Theta})$ can be partitioned as

$$\mathbf{I}(\boldsymbol{\Theta}) = \begin{bmatrix}\mathbf{I}_{\boldsymbol{\Theta}_r,\boldsymbol{\Theta}_r}(\boldsymbol{\Theta}) & \mathbf{I}_{\boldsymbol{\Theta}_r,\boldsymbol{\Theta}_s}(\boldsymbol{\Theta})\\ \mathbf{I}_{\boldsymbol{\Theta}_s,\boldsymbol{\Theta}_r}(\boldsymbol{\Theta}) & \mathbf{I}_{\boldsymbol{\Theta}_s,\boldsymbol{\Theta}_s}(\boldsymbol{\Theta})\end{bmatrix} \tag{20}$$

Based on the matrix inversion formula [42], we can derive

$$\left[\mathbf{I}^{-1}(\boldsymbol{\Theta})\right]_{\boldsymbol{\Theta}_r,\boldsymbol{\Theta}_r} = \left[\mathbf{I}_{\boldsymbol{\Theta}_r,\boldsymbol{\Theta}_r}(\boldsymbol{\Theta}) - \mathbf{I}_{\boldsymbol{\Theta}_r,\boldsymbol{\Theta}_s}(\boldsymbol{\Theta})\mathbf{I}^{-1}_{\boldsymbol{\Theta}_s,\boldsymbol{\Theta}_s}(\boldsymbol{\Theta})\mathbf{I}_{\boldsymbol{\Theta}_s,\boldsymbol{\Theta}_r}(\boldsymbol{\Theta})\right]^{-1} \tag{21}$$

Noting the independence between component $\boldsymbol{\Theta}_r$ and $\boldsymbol{\Theta}_s$, we have $\mathbf{I}_{\boldsymbol{\Theta}_r,\boldsymbol{\Theta}_s}(\boldsymbol{\Theta}) = \mathbf{0}$. Thus, (21) can be reformulated as

$$\left[\mathbf{I}^{-1}(\boldsymbol{\Theta})\right]_{\boldsymbol{\Theta}_r,\boldsymbol{\Theta}_r} = \left[\mathbf{I}_{\boldsymbol{\Theta}_r,\boldsymbol{\Theta}_r}(\boldsymbol{\Theta})\right]^{-1} \tag{22}$$

Differentiating the logarithm of (9) w.r.t $\boldsymbol{\Theta}_r^*$ results in:

$$\frac{\partial \ln f_1(\mathbf{Z}_p|\boldsymbol{\Theta})}{\partial \boldsymbol{\Theta}_r^*} = \begin{bmatrix}\frac{\mathbf{U}^H\mathbf{M}^{-1}(\mathbf{z}_{p1}-\mathbf{U}\mathbf{b}_{p1})}{\tau_1},\\ \frac{\mathbf{U}^H\mathbf{M}^{-1}(\mathbf{z}_{p2}-\mathbf{U}\mathbf{b}_{p2})}{\tau_2},\\ \cdots,\\ \frac{\mathbf{U}^H\mathbf{M}^{-1}(\mathbf{z}_{pK}-\mathbf{U}\mathbf{b}_{pK})}{\tau_K}\end{bmatrix}^T \tag{23}$$

By substituting (11) and (23) into (19), we can obtain.

$$\begin{aligned}\mathbf{I}_{\boldsymbol{\Theta}_r,\boldsymbol{\Theta}_r}(\hat{\boldsymbol{\Theta}}_0) &= E\left\{\left[\frac{\partial \ln f_1(\mathbf{Z}_p|\boldsymbol{\Theta})}{\partial \boldsymbol{\Theta}_r^*}\right]\left[\frac{\partial \ln f_1(\mathbf{Z}_p|\boldsymbol{\Theta})}{\partial \boldsymbol{\Theta}_r^T}\right]\right\}\\ &= \mathbf{U}^H\mathbf{M}^{-1}\mathbf{U}\cdot\mathrm{diag}\left(\frac{4}{\hat{\tau}_{1,0}}, \frac{4}{\hat{\tau}_{2,0}}, \ldots, \frac{4}{\hat{\tau}_{K,0}}\right)\end{aligned} \tag{24}$$

Then, it can be derived from (22) and (24) that:

$$\left[\mathbf{I}^{-1}(\hat{\boldsymbol{\Theta}}_0)\right]_{\boldsymbol{\Theta}_r,\boldsymbol{\Theta}_r} = \operatorname{diag}\left(\frac{\hat{\tau}_{1,0}}{4}, \frac{\hat{\tau}_{2,0}}{4}, \ldots, \frac{\hat{\tau}_{K,0}}{4}\right)\left(\mathbf{U}^H\mathbf{M}^{-1}\mathbf{U}\right)^{-1} \tag{25}$$

Plugging (12), (16), (23) and (25) into (18) and simplifying the result, we can obtain the Rao test as

$$\lambda_{\text{Rao}} = \sum_{k=1}^{K} \frac{(N+q_k+1)\operatorname{tr}\left(\mathbf{z}_{pk}^H\mathbf{P}_U\mathbf{z}_{pk}\right)}{\operatorname{tr}\left(\mathbf{z}_{pk}^H\mathbf{M}^{-1}\mathbf{z}_{pk}\right)+\beta_k} \tag{26}$$

Comparing (17) and (26), it can be found that for the hypothesis testing problem in (4), the detection statistic based on the two-step Rao criterion is consistent with that based on the two-step Gradient criterion. Given this equivalence, the subsequent analysis will primarily focus on the performance of the Gradient-based detector.

3.2.3 *Wald test for known M*

The detection statistic based on the two-step Wald criterion for the detection problem indicated in (4) can be formulated as

$$\lambda_{\text{Wald}} = \left(\hat{\boldsymbol{\Theta}}_{r1}-\boldsymbol{\Theta}_{r0}\right)^H\left[\mathbf{I}^{-1}\left(\hat{\boldsymbol{\Theta}}_1\right)_{\boldsymbol{\Theta}_r,\boldsymbol{\Theta}_r}\right]^{-1}\left(\hat{\boldsymbol{\Theta}}_{r1}-\boldsymbol{\Theta}_{r0}\right) \tag{27}$$

with $\hat{\boldsymbol{\Theta}}_1$ being the ML estimate of $\boldsymbol{\Theta}$ under H_1. Note that $\boldsymbol{\Theta}_{r0} = \mathbf{0}_{2rK\times 1}$. Similar to (24), we can derive

$$\mathbf{I}_{\boldsymbol{\Theta}_r,\boldsymbol{\Theta}_r}\left(\hat{\boldsymbol{\Theta}}_1\right) = \mathbf{U}^H\mathbf{M}^{-1}\mathbf{U}\cdot\operatorname{diag}\left(\frac{4}{\hat{\tau}_{1,1}}, \frac{4}{\hat{\tau}_{2,1}}, \ldots, \frac{4}{\hat{\tau}_{K,1}}\right) \tag{28}$$

where $\hat{\tau}_{k,1}, k=1,2,\ldots,K$ denotes the estimated value of τ_k under H_1. And the MAP PDF of τ_k under H_1 can be expressed as:

$$f_1\left(\tau_k|\boldsymbol{Z}_p\right) = \frac{f_1\left(\boldsymbol{Z}_p|\boldsymbol{\Theta}\right)f\left(\tau_k\right)}{f_1\left(\boldsymbol{Z}_p\right)} \tag{29}$$

where $f_1\left(\boldsymbol{Z}_p\right) = \int f_1\left(\boldsymbol{Z}_p|\boldsymbol{\Theta}\right)f\left(\tau_1\right)f\left(\tau_2\right)\cdots f\left(\tau_K\right)d\boldsymbol{\Theta}_s$ denotes the PDF of $\boldsymbol{Z}_p$ under H_1.

By taking the derivative of $f_1\left(\tau_k|\boldsymbol{Z}_p\right)$ w.r.t τ_k and equating it to zero, we can derive the MAP estimate of τ_k under H_1:

$$\begin{aligned}\hat{\tau}_{k,1} &= \arg\max_{\tau_k} f_1\left(\boldsymbol{Z}_p|\boldsymbol{\Theta}\right)f\left(\tau_k\right)\\ &= \frac{\operatorname{tr}\left[\left(\mathbf{z}_{pk}-\mathbf{U}\mathbf{b}_{pk}\right)^H\mathbf{M}^{-1}\left(\mathbf{z}_{pk}-\mathbf{U}\mathbf{b}_{pk}\right)\right]+\beta_k}{N+q_k+1}\end{aligned} \tag{30}$$

Note that $\boldsymbol{\Theta}_{r0} = \mathbf{0}_{2rK\times 1}$. By substituting (14), (28), and (30) into (27) and subsequently simplifying the result, we arrive at the Wald test:

$$\lambda_{\text{Wald}} = \sum_{k=1}^{K} \frac{(N+q_k+1)\operatorname{tr}\left(\mathbf{z}_{pk}^H\mathbf{P}_U\mathbf{z}_{pk}\right)}{\operatorname{tr}\left(\mathbf{z}_{pk}^H\mathbf{P}_U^{\perp}\mathbf{z}_{pk}\right)+\beta_k} \tag{31}$$

with $\mathbf{P}_U^{\perp} = \mathbf{M}^{-1}-\mathbf{P}_U$.

3.3 Implementation of Adaptive Detector for unknown M

In practice, the CCM $\mathbf{M}$ is always unknown and should be approximated based on the training data. Subsequently, we utilize the persymmetric FP estimate of CCM to replace the unknown $\mathbf{M}$ in the detection statistic derived in subsection 3.2. Specifically, the FP estimate of CCM can be obtained by [43]:

$$\hat{\mathbf{M}}_{\text{FP}}^{(i+1)} = \frac{N}{R}\sum_{l=1}^{R}\frac{\mathbf{y}_l\mathbf{y}_l^{\text{H}}}{\mathbf{y}_l^{\text{H}}(\hat{\mathbf{M}}_{\text{FP}}^{(i)})^{-1}\mathbf{y}_l} \tag{32}$$

where $\hat{\mathbf{M}}_{\text{FP}}^{(i)}$ represents the tth iterated estimate. The initial value is set as $\hat{\mathbf{M}}_{\text{FP}}^{(0)} = \frac{N}{R}\sum_{l=1}^{R}\frac{\mathbf{y}_l\mathbf{y}_l^{\text{H}}}{\mathbf{y}_l^{\text{H}}\mathbf{y}_l}$, and the final iteration result is denoted by $\hat{\mathbf{M}}_{\text{FP}}^{(t)}$, where t represents the number of iterations. Integrating the persymmetry [44] into the estimate in (32) results in the persymmetric FP estimate:

$$\hat{\mathbf{M}}_{\text{PFP}} = \frac{1}{2}\left(\hat{\mathbf{M}}_{\text{FP}}^{(t)}+\mathbf{D}_N(\hat{\mathbf{M}}_{\text{FP}}^{(t)})^*\mathbf{D}_N\right) \tag{33}$$

Replacing the unknown $\mathbf{M}$ in (17) and (31) by $\hat{\mathbf{M}}_{\text{PFP}}$ in (33), we can obtain the final adaptive statistics of the Gradient (or Rao equivalently) and Wald tests (notated as PS-Gradient-iGCG and PS-Wald-iGCG) as follows:

$$\begin{aligned}\lambda_{\text{PS-Gradient-iGCG}} &= \lambda_{\text{PS-Rao-iGCG}}\\ &= \sum_{k=1}^{K}\frac{(N+q_k+1)\operatorname{tr}\left(\mathbf{z}_{pk}^{\text{H}}\mathbf{P}_{\bar{U}}\mathbf{z}_{pk}\right)}{\operatorname{tr}\left(\mathbf{z}_{pk}^{\text{H}}\hat{\mathbf{M}}_{\text{PFP}}^{-1}\mathbf{z}_{pk}\right)+\beta_k}\end{aligned} \tag{34}$$

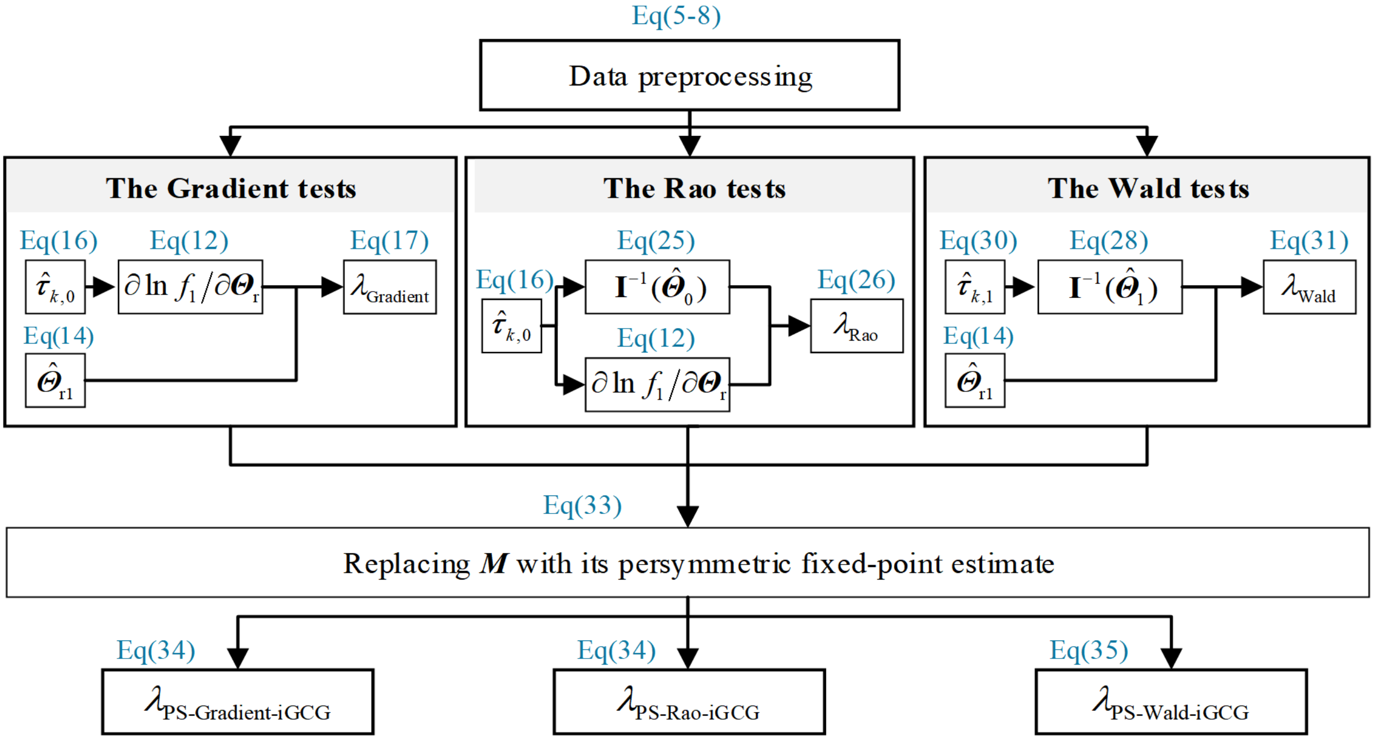

Figure 1. Illustrative flowchart of derivation.

Table 1. Distribution of energy among various MDS models.

Model	The number of range cell						
	1	2	$\cdots$	h_0-1	h_0	$\cdots$	K
Model 1	$1/h_0$	$1/h_0$	$1/h_0$	$1/h_0$	0	0	$1/h_0$
Model 2	0.5	$0.5/(h_0-1)$	$0.5/(h_0-1)$	$0.5/(h_0-1)$	0	0	$0.5/(h_0-1)$
Model 3	0.9	$0.1/(h_0-1)$	$0.1/(h_0-1)$	$0.1/(h_0-1)$	0	0	$0.1/(h_0-1)$
Model 4	1	0	0	0	0	0	0

and

$$\lambda_{\text{PS-Wald-iGCG}} = \sum_{k=1}^{K} \frac{(N+q_k+1)\,\mathrm{tr}\left(\mathbf{z}_{pk}^H \mathbf{P}_{\bar{U}} \mathbf{z}_{pk}\right)}{\mathrm{tr}\left(\mathbf{z}_{pk}^H \mathbf{P}_{\bar{U}}^{\perp} \mathbf{z}_{pk}\right) + \beta_k} \tag{35}$$

where $\mathbf{P}_{\bar{U}}^{\perp} = \hat{\mathbf{M}}_{\text{PFP}}^{-1} - P_U$ with $\mathbf{P}_U = \hat{\mathbf{M}}_{\text{PFP}}^{-1}\mathbf{U}\left(\mathbf{U}^H\hat{\mathbf{M}}_{\text{PFP}}^{-1}\mathbf{U}\right)^{-1}\mathbf{U}^H\hat{\mathbf{M}}_{\text{PFP}}^{-1}$.

The proposed detectors can be viewed as a novel information fusion scheme, which coherently combines the information from multiple range cells to enhance the detection performance. To clearly illustrate the sequence of parameter estimation, we have provided Figure 1. Additionally, it is worth noting that all three proposed detectors possess the asymptotically CFAR property. For detailed theoretical proofs, please refer to Appendix.

4 Numerical results

In this section, we perform Monte Carlo simulations to assess the efficacy of the proposed detectors. Due to the equivalence between PS-Gradient-iGCG and PS-Rao-iGCG, this section will focus on analyzing the detection performance of PS-Gradient-iGCG and PS-Wald-iGCG. We conduct 10^4 and 10^5 independent trials to ascertain the probability of detection (P_d) and the threshold, respectively, for a specified probability of false alarm $P_{fa} = 10^{-3}$. Balancing the requirements for estimation accuracy and computational complexity, the number of iterations for CCM estimation is set to $t = 3$. Moreover, the non-zero matrices $\mathbf{U}$ is generated randomly for the purpose of the simulations, and the element located at the i^{th} row and the j^{th} column of $\mathbf{M}$ can be expressed as $[\mathbf{M}]_{i,j} = \rho^{|i-j|}, \quad 1 \le i,j \le N$ where ρ signifies the one-lag correlation coefficient of clutter. And the shape parameter q_k and the scale parameter β_k for the texture component are generated randomly.

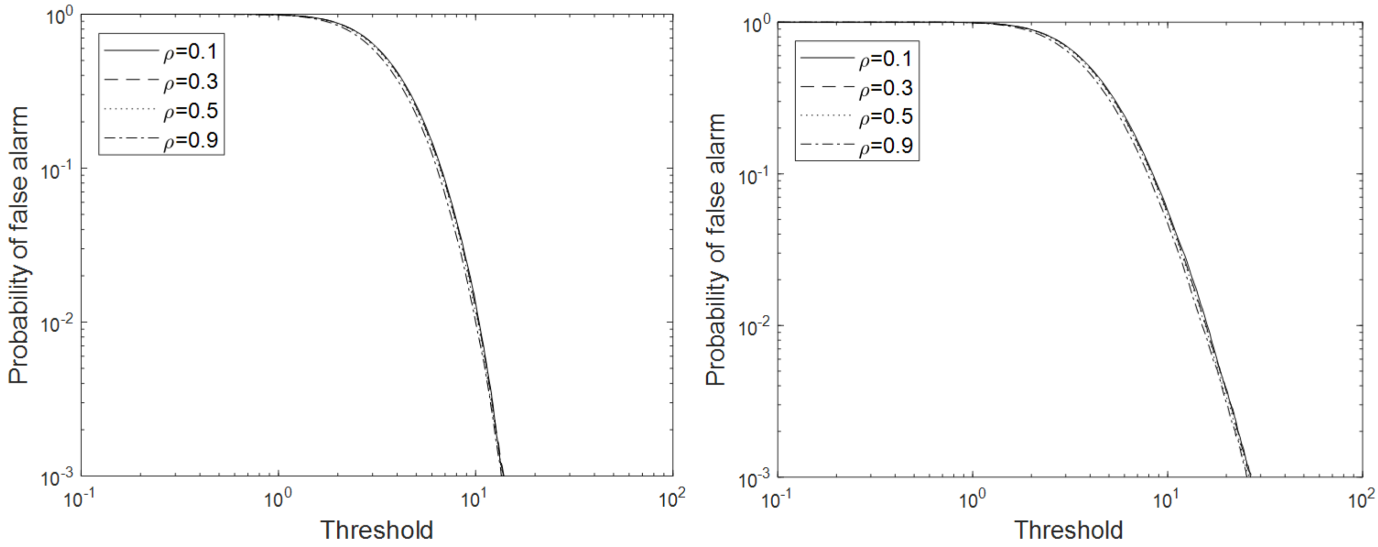

(a) PS-Gradient-iGCG (b) PS-Wald-iGCG

Figure 2. P_{fa} vs. threshold for $N = 8, K = 5, R = 12, r = 3, \rho = 0.1, 0.3, 0.5, 0.9, h_0 = 3, q = 3, \beta = 4$.

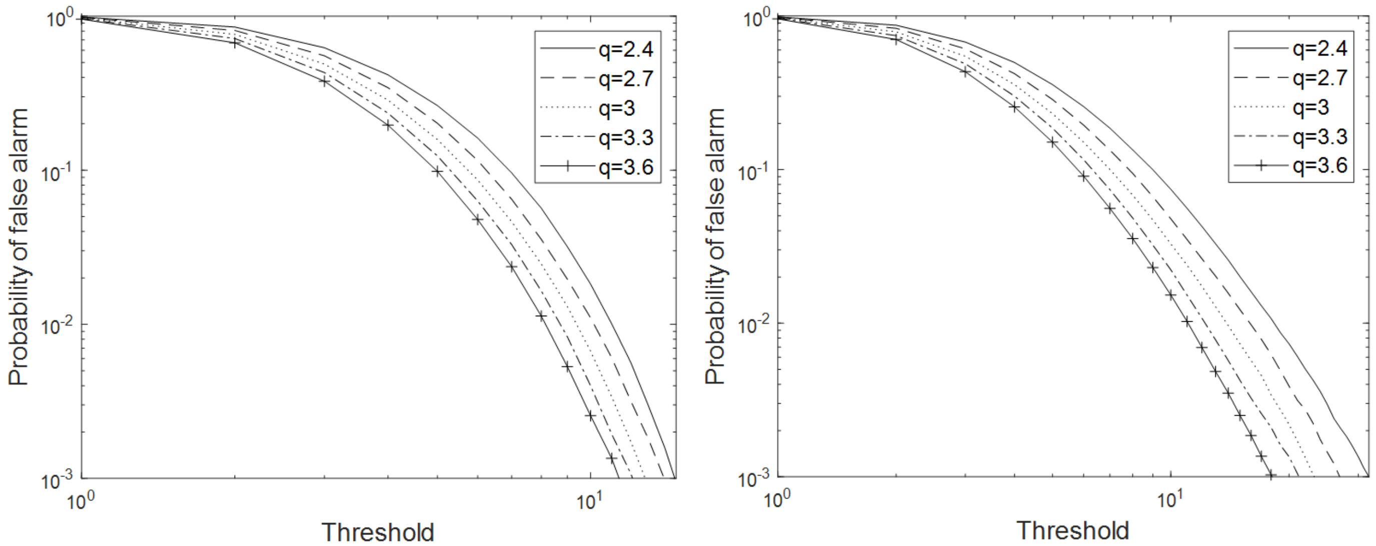

(a) PS-Gradient-iGCG (b) PS-Wald-iGCG

Figure 3. P_{fa} vs. threshold for $N = 8, K = 5, R = 12, r = 3, \rho = 0.9, h_0 = 3, q = 2.4, 2.7, 3, 3.3, 3.6, \beta = 4$.

Furthermore, the signal-to-clutter ratio (SCR) is defined as:

$$\mathrm{SCR} = \frac{1}{K \cdot E(\tau)} \sum_{k=1}^{K} \mathbf{b}_k^H \mathbf{U}^H \mathbf{M}^{-1} \mathbf{U} \mathbf{b}_k \tag{36}$$

Additionally, Table 1 showcases four illustrative examples of multiple dominant scatterers (MDS), emphasizing that within the range of K cells, only h_0 cells contain target signal components.

For the sake of simplicity and clarity, unless stated otherwise, the shape parameters $q_k, k = 1, 2, \ldots, K+R$ and scale parameters $\beta_k, k = 1, 2, \ldots, K+R$ are set to be identical across all range cells, i.e., $q = q_1 = q_2 = \cdots = q_{K+R}$ and $\beta = \beta_1 = \beta_2 = \cdots = \beta_{K+R}$.

4.1 Asymptotically CFAR evaluation

To verify that the proposed detectors exhibit the asymptotically CFAR characteristic, Figure 2 depict the correlation between P_{fa} and the detection threshold across various configurations of ρ. Notably, the four curves, each embodying distinct parameter sets, exhibit negligible separation, indicating that the both detectors of PS-Rao-iGCG and PS-Gradient-iGCG retain the asymptotic CFAR property.

Moreover, Figures 3 and 4 provide further detail on

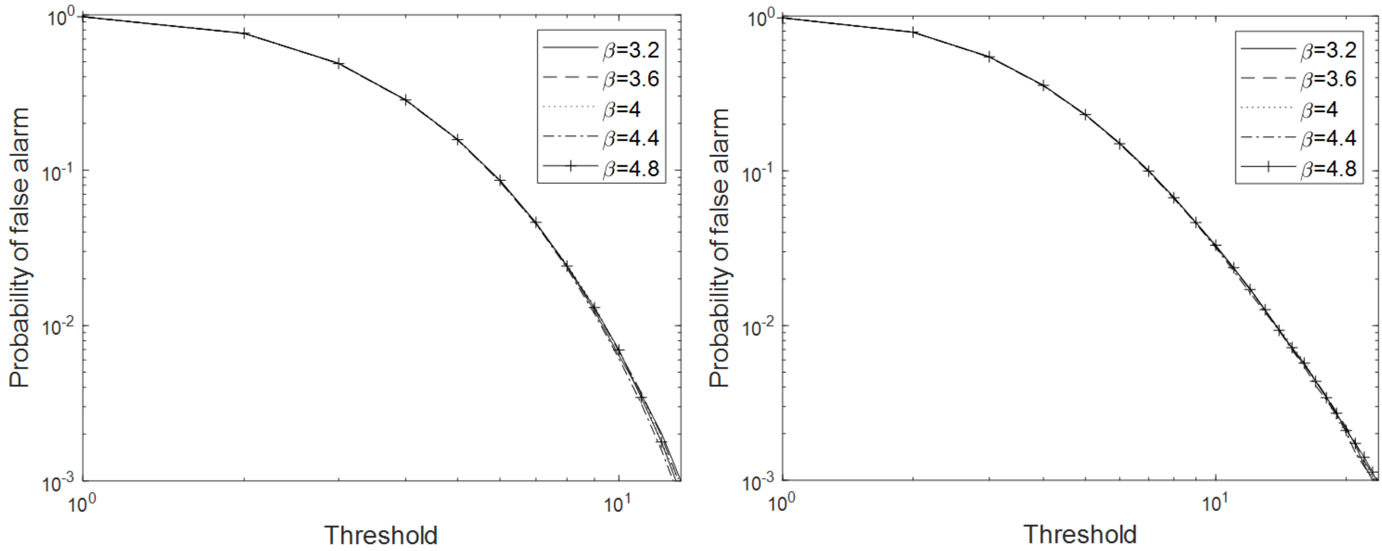

(a) PS-Gradient-iGCG

(b) PS-Wald-iGCG

Figure 4. P_{fa} vs. threshold for $N = 8, K = 5, R = 12, r = 3, \rho = 0.9, h_0 = 3, q = 3, \beta = 3.2, 3.6, 4, 4.4, 4.8$.

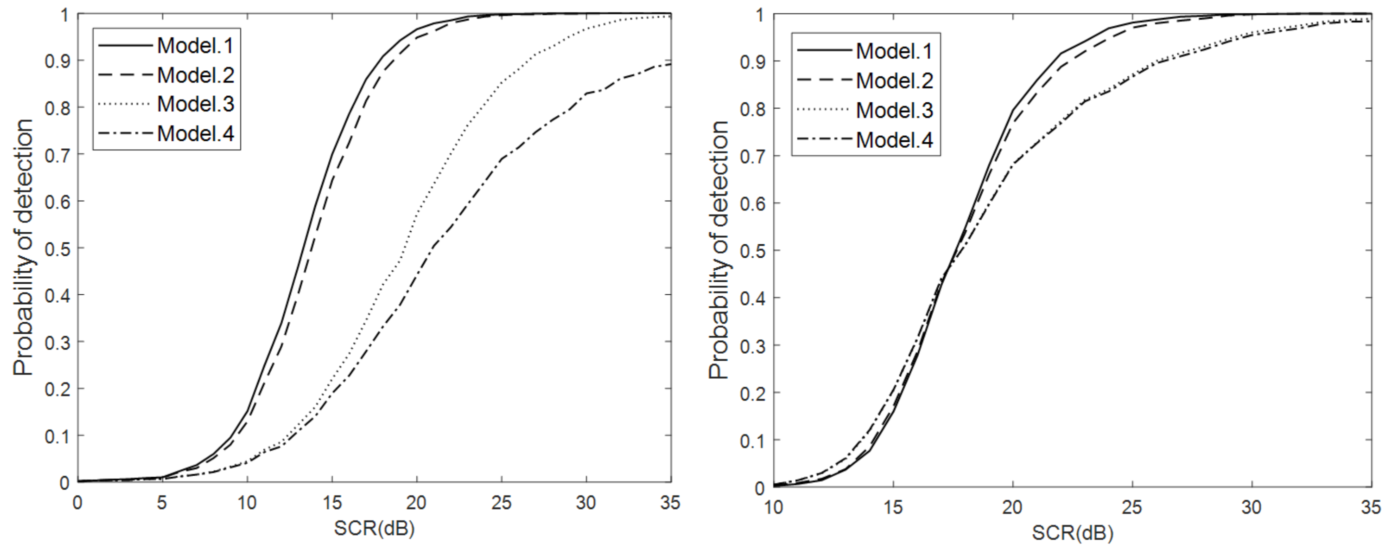

(a) PS-Gradient-iGCG

(b) PS-Wald-iGCG

Figure 5. P_d vs. SCR with Model.1-4 for $N = 8, K = 5, R = 12, r = 3, \rho = 0.9, h_0 = 3, q = 3, \beta = 4$.

how the P_{fa} and detection threshold vary with changes in the shape and scale parameters of the texture, respectively. The results show that the proposed detectors exhibit CFAR behavior w.r.t to the scale parameter, but does not maintain CFAR properties under variations in the shape parameter.

4.2 Effect of parameters on the proposed detectors

Figure 5 displays the plots of P_d against SCR for four representative MDS models listed in Table 1. It is evident that when the target signal energy is evenly distributed across multiple range cells (as defined in Model.1), the proposed detectors achieve peak detection capability. Conversely, a significant concentration of target energy within a single range cell leads to measurable performance degradation, a phenomenon termed "collapsing loss" [45]. For consistency, all subsequent analyses will adopt the energy distribution framework outlined in Model.1 unless explicitly stated otherwise. Moreover, Figure 6 displays the curves illustrating the relationship between P_d and SCR for various values of h_0 ($h_0 = 1, 2, 3, 4$). The results demonstrate that as the values of h_0 rise, the performance of the proposed detectors improves.

In Figure 7, the detection capabilities of the proposed detectors are exhibited across various clutter one-lag correlation coefficients. The closely aligned curves

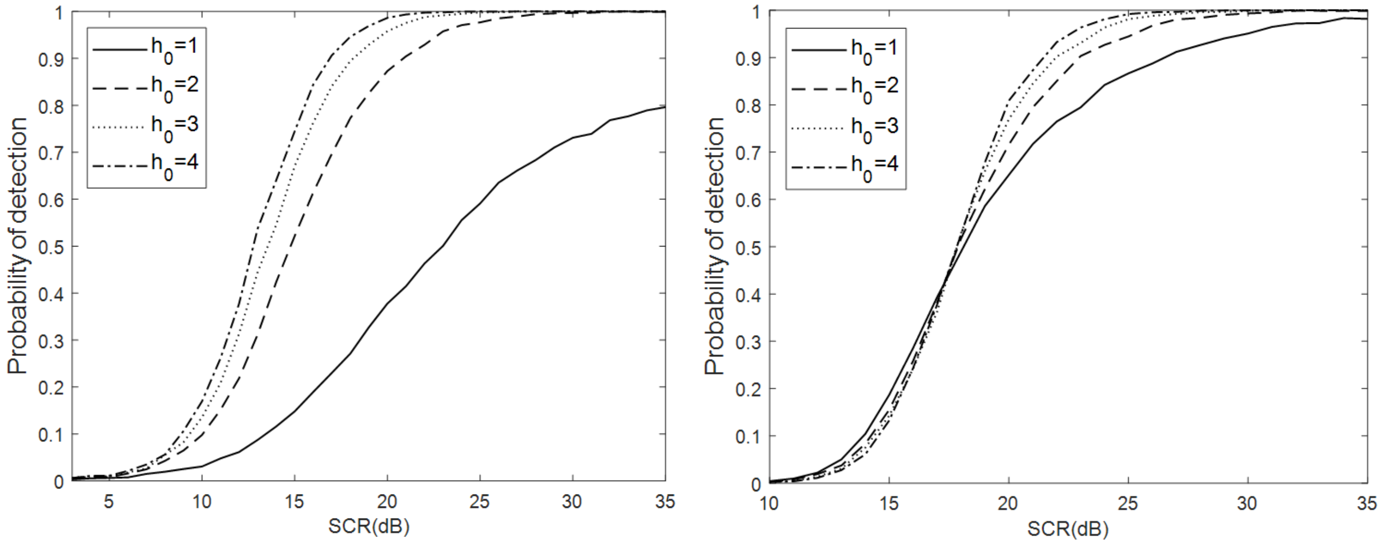

(a) PS-Gradient-iGCG (b) PS-Wald-iGCG

Figure 6. P_d vs. SCR with Model.1-4 for $N=8, K=5, R=12, r=3, \rho=0.9, h_0=1,2,3,4, q=3, \beta=4$.

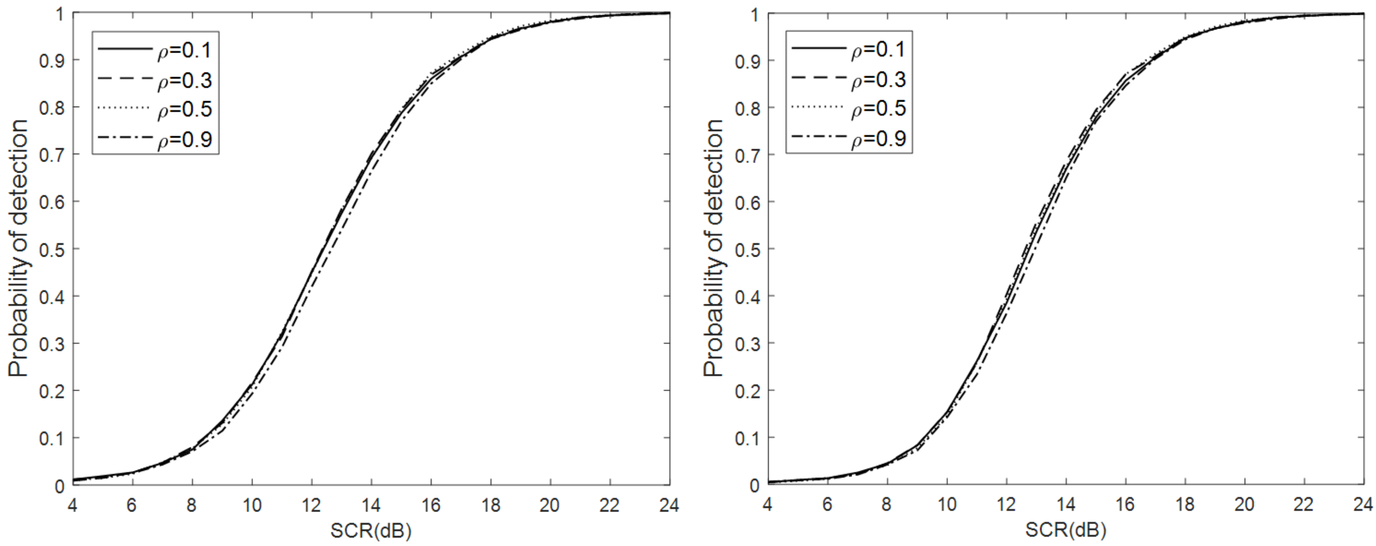

(a) PS-Gradient-iGCG (b) PS-Wald-iGCG

Figure 7. P_d vs. SCR with Model.1-4 for $N=8, K=5, R=12, r=3, \rho=0.1,0.3,0.5,0.9, h_0=3, q=3, \beta=4$.

indicate that detectors maintain robust performance regardless of the clutter correlation. In addition, Figure 8 demonstrates the detection performance of the proposed detectors for different values of N and R. Specifically, when R is fixed at 12, the performance of the detectors decreases as N increases. This decline can be explained by the fact that the dimension of the unknown parameter in $\mathbf{M}$ scales with N. When the training data size is fixed, a larger value of N results in reduced estimation accuracy for $\mathbf{M}$, negatively impacting detection performance. Conversely, the results indicate that for a fixed $N=12$, enhancing detection performance is possible by increasing R, as a larger training dataset allows for a more accurate estimation of the unknown $\mathbf{M}$.

4.3 Comparison of performance among various detectors

We compare the proposed PS-Gradient-iGCG and PS-Wald-iGCG with other existing non-persymmetric subspace detectors, namely S-GLRT-CG [24], S-Rao-CG [24], and S-Wald-CG [24] (note that S-Gradient-CG and S-Durbin-CG are not considered as they are equivalent to S-Rao-CG, as mentioned in the introduction). Additionally, we also compare them with the existing persymmetric detectors including P-Rao-iGCG [37] and P-Wald-iGCG [37].

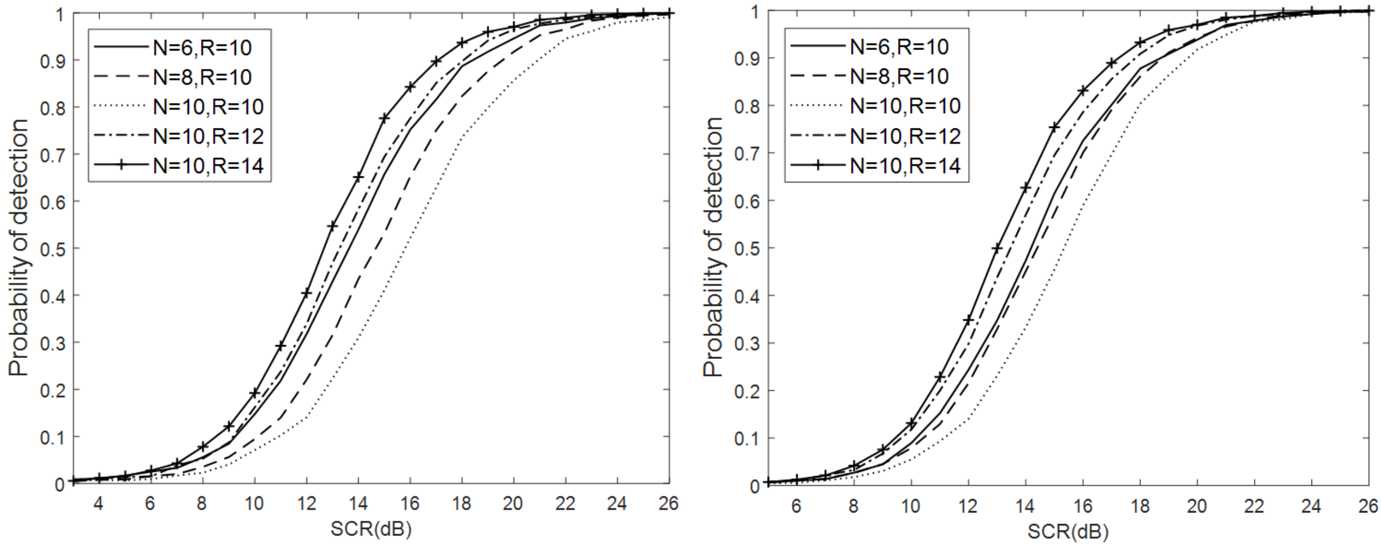

(a) PS-Gradient-iGCG (b) PS-Wald-iGCG

Figure 8. P_d vs. SCR with Model.1-4 for $N = 6, 8, 10, K = 5, R = 10, 12, 14, r = 3, \rho = 0.9, h_0 = 3, q = 3, \beta = 4$.

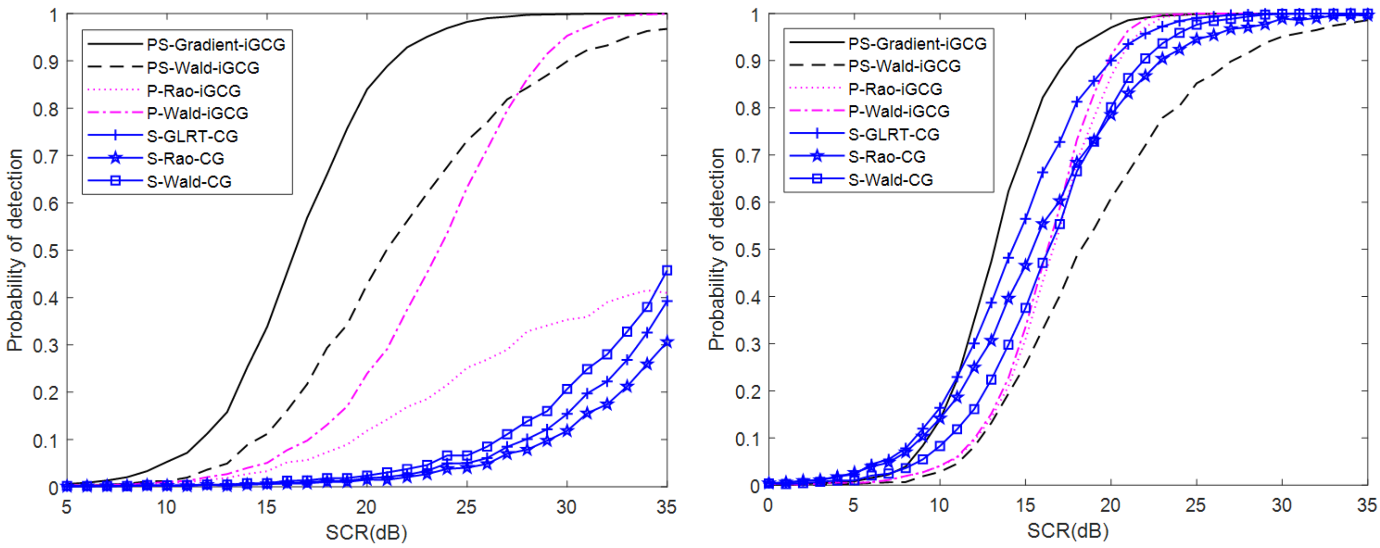

(a) R=8 (b) R=16

Figure 9. P_d vs. SCR for $N = 8, K = 5, R = 8, 16, r = 3, \rho = 0.9, h_0 = 3, q = 3, \beta = 4$.

Figure 9 contrasts the performance of the proposed detectors with that of competitors across various values of R. It is evident from the Figure 9 that the proposed PS-Gradient-iGCG surpasses other detectors, particularly when training data is scarce. Furthermore, as the amount of training data increases, the performance gap between the non-persymmetric detectors and the persymmetric ones narrows. This suggests that exploiting the persymmetric structure of the CCM can yield a significant enhancement in detection performance, especially when training data is limited. However, when a sufficient amount of training data is available, the CCM can be estimated accurately without necessarily leveraging the persymmetry.

Additionally, Figure 10 demonstrates the P_d for various detectors as a function of R, with a constant SCR $= 15\,\mathrm{dB}$. The results clearly indicate that the proposed PS-Gradient-iGCG outperforms its counterparts, especially in scenarios where the training dataset is limited in size.

However, in real-world applications, various factors like wavefront distortions and errors in array calibration can lead to deviations between the nominal signal subspace matrix $\mathbf{U}$ and the actual signal subspace matrix $\tilde{U}$. Subsequent discussions will focus on such mismatch scenarios. The angle of mismatch

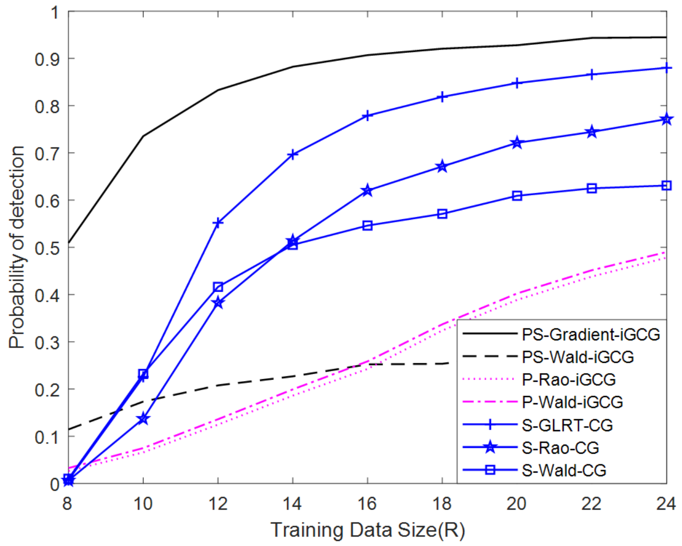

Figure 10. P_d vs. R for $N = 8, K = 5, r = 3, \rho = 0.9, h_0 = 3, q = 3, \beta = 4, SCR = 15dB$.

(denoted as φ) is defined as [46]:

$$\cos^2 \varphi = \frac{\left| \mathrm{tr}(\tilde{\mathbf{U}}\mathbf{M}^{-1}\mathbf{U}) \right|^2}{\mathrm{tr}(\tilde{\mathbf{U}}\mathbf{M}^{-1}\tilde{\mathbf{U}})\,\mathrm{tr}(\mathbf{U}\mathbf{M}^{-1}\mathbf{U})} \tag{37}$$

When there is a mismatch, the ratio of signal to clutter is characterized as follows:

$$\mathrm{SCR}' = \frac{1}{K \cdot E(\tau)} \sum_{k=1}^{K} \mathbf{b}_k^H \tilde{\mathbf{U}}^H \mathbf{M}^{-1} \tilde{\mathbf{U}} b_k \tag{38}$$

The detection performance of different detectors under moderate signal mismatch ($\cos^2 \varphi = 0.5$) is visualized for different values of R in Figure 11 through P_d vs. SCR' curves. Experimental findings reveal that the proposed algorithms, especially the PS-Gradient-iGCG, maintain enhanced effectiveness against signal mismatch. Figure 12 further analyzes the relationship between P_d and $\cos^2 \varphi$ for a given value of SCR', consistently demonstrating the superiority of PS-Gradient-iGCG and PS-Wald-iGCG in multiple mismatch scenarios. For clearer visualization, Figure 13 presents showcases mesa plots that depict constant P_d for selected detectors, including PS-Gradient-iGCG, PS-Wald-iGCG, S-Wald-CG, and P-Wald-iGCG, which showed relatively stable performance in preceding analyses. It is evident that all detectors require incremental SCR' adjustments to maintain equivalent P_d as mismatch levels increase. Notably, the designed PS-Gradient-iGCG exhibits the smallest variation in SCR' compared to the counterparts, indicating its enhanced adaptability.

To demonstrate the effectiveness of the proposed detectors, we evaluated their performance using real sea clutter data collected by the IPIX radar in 1998 [47]. The key parameters of the selected dataset are provided in Table 2. As illustrated in Figure 14, the proposed detectors exhibit superior detection performance compared to other methods under both matched and mismatched conditions.

Table 2. Real data parameters.

File name	Range resolution	Range cells
19980205_171203_ANTSTEP	30m	28

5 Conclusion

This paper addresses the challenge of adaptively detecting range-spread targets embedded within compound-Gaussian clutter characterized by inverse-Gamma textures and an unknown CCM. Specifically, the target signals are presumed to be deterministic and confined within a predefined subspace, albeit with unknown coordinates. Leveraging the persymmetry of the CCM, we have devised three detectors including PS-Gradient-iGCG, PS-Rao-iGCG and PS-Wald-iGCG, which all exhibit the asymptotic CFAR characteristics relative to the unknown speckle covariance matrix structure, and the robustness of three proposed detectors under different clutter correlation scenarios is confirmed through Monte Carlo simulations. Interestingly, two designed detectors PS-Gradient-iGCG and PS-Rao-iGCG are found to be equivalent theoretically. And both of them outperform the developed PS-Wald-iGCG in terms of match and mismatch cases. Furthermore, the proposed detectors demonstrate superior performance compared to existing methods, particularly in scenarios with limited training data. With further development and optimization, the proposed methods could be applied to maritime wideband radar target detection under clutter-heavy environments, as well as in the detection of spatially close point-like targets moving at similar velocities.

Appendix: CFAR behaviors of the proposed detectors

The asymptotically CFAR property serves as a crucial indicator for evaluating the adaptive performance of the detectors. Following, we will theoretically demonstrate the asymptotically CFAR characteristic of the PS-Gradient-iGCG (or equivalent PS-Rao-iGCG) and PS-Wald-iGCG w.r.t the structure of the unknown CCM.

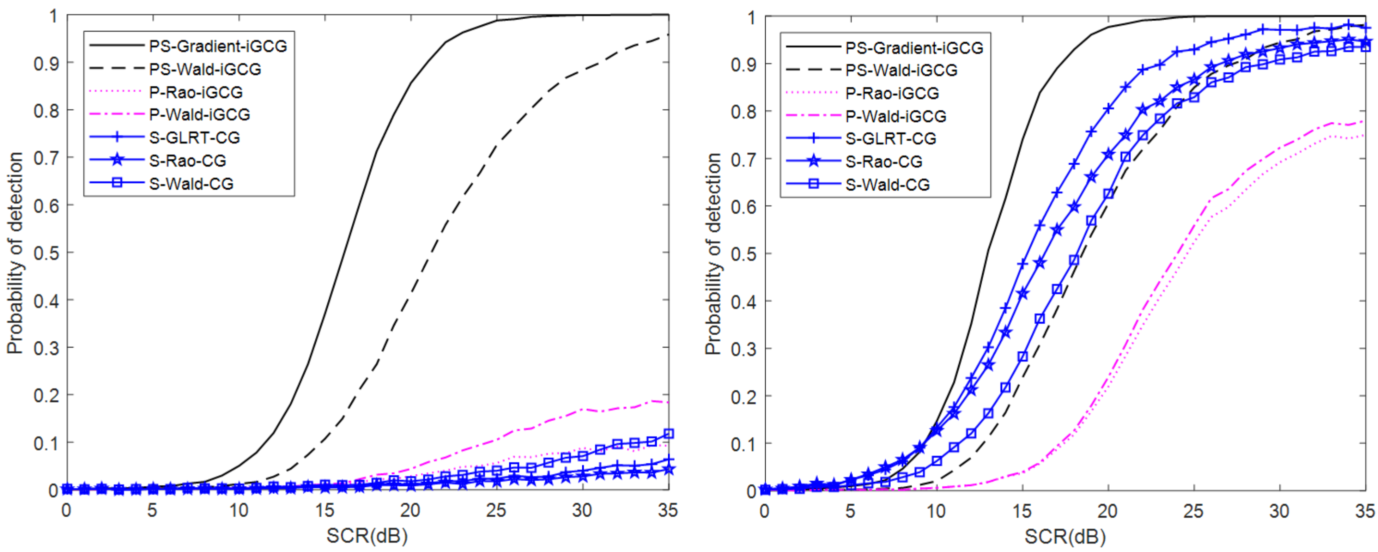

(a) R=8 (b) R=16

Figure 11. P_d vs. SCR for $N=8, K=5, R=8,16, r=3, \rho=0.9, h_0=3, q=3, \beta=4$.

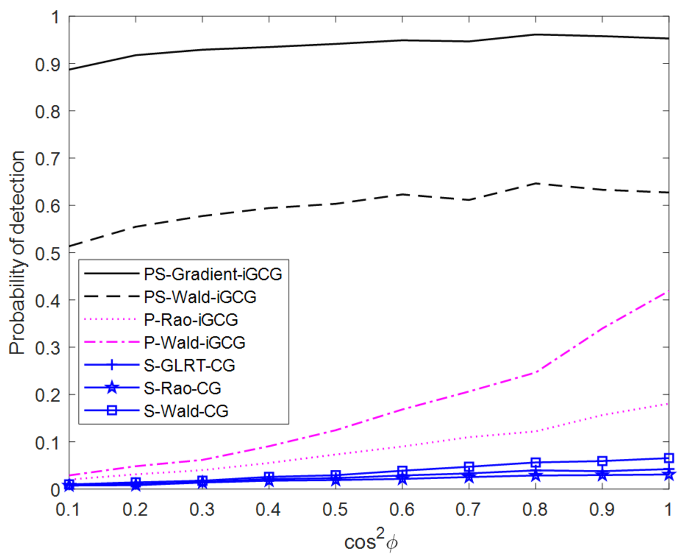

Figure 12. P_d vs. $cos^2\phi$ for $N=8, K=5, R=12, r=3, \rho=0.9, h_0=3, q=3, \beta=4, SCR'=23dB$.

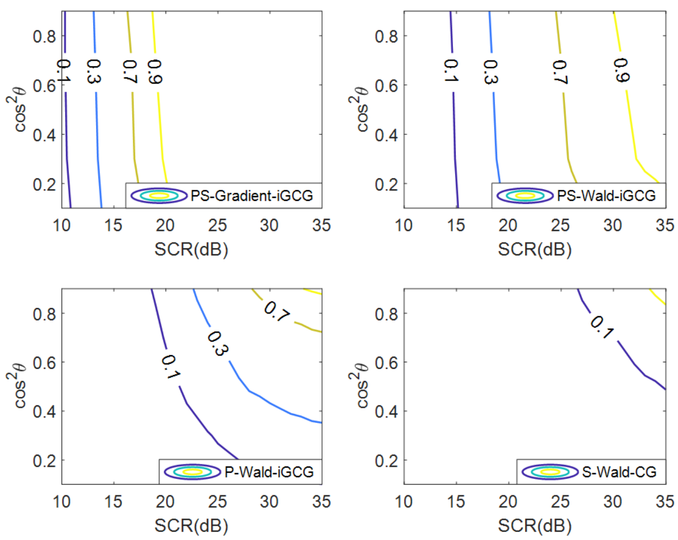

Figure 13. Mesa plots of constant P_d for $N=8, K=5, R=8, r=3, \rho=0.9, h_0=3, q=3, \beta=4$.

From (34) and (35), it is evident that, in order to prove the asymptotically CFAR property of the proposed detectors, it suffices to demonstrate that as $n\to\infty$, the asymptotic statistical properties of the components $\mathbf{z}_{pk}^H\hat{\mathbf{M}}_{\mathrm{PFP}}^{-1}\mathbf{z}_{pk}$ and $\mathbf{z}_{pk}^H\mathbf{P}_{\bar{U}}\mathbf{z}_{pk}$ are independent of $\mathbf{M}$ under H_0.

First, we rewrite $\mathbf{z}_{pk}^H\hat{\mathbf{M}}_{\mathrm{PFP}}^{-1}\mathbf{z}_{pk}$ and $\mathbf{z}_{pk}^H\mathbf{P}_{\bar{U}}\mathbf{z}_{pk}$ as

$$\begin{cases}\mathbf{z}_{pk}^H\hat{\mathbf{M}}_{\mathrm{PFP}}^{-1}\mathbf{z}_{pk}=\bar{\mathbf{z}}_{pk}^H\overline{\mathbf{M}}_{\mathrm{PFP}}^{-1}\bar{\mathbf{z}}_{pk}\\ \mathbf{z}_{pk}^H P_{\bar{U}}^{\perp}\mathbf{z}_{pk}=\bar{\mathbf{z}}_{pk}^H\overline{\mathbf{P}}\bar{\mathbf{z}}_{pk}\end{cases}\tag{A.1}$$

with

$$\begin{cases}\bar{\mathbf{z}}_{pk}=\mathbf{M}^{-1/2}\mathbf{z}_{pk}\\ \overline{\mathbf{M}}_{\mathrm{PFP}}=\mathbf{M}^{-1/2}\hat{\mathbf{M}}_{\mathrm{PFP}}M^{-1/2}\\ \overline{\mathbf{U}}=\mathbf{M}^{-1/2}\mathbf{U}\\ \overline{\mathbf{P}}=\overline{\mathbf{M}}_{\mathrm{PFP}}^{-1}-\overline{\mathbf{M}}_{\mathrm{PFP}}^{-1}\overline{\mathbf{U}}(\overline{\mathbf{U}}^H\overline{\mathbf{M}}_{\mathrm{PFP}}^{-1}\overline{\mathbf{U}})^{-1}\overline{\mathbf{U}}^H\overline{\mathbf{M}}_{\mathrm{PFP}}^{-1}\end{cases}\tag{A.2}$$

Certainly, under H_0, we have $\bar{\mathbf{z}}_{pk}\sim\mathbf{CN}(\mathbf{0}_{N\times 2},\mathbf{I}_N)$ after whitening by the true covariance matrix $\mathbf{M}$. Furthermore, when the final iteration count reaches $n\to\infty$, $\overline{\mathbf{M}}_{\mathrm{PFP}}\sim\mathbf{CW}(2R,\mathbf{I}_N)$. Consequently, from (A.1), under H_0, the asymptotic statistical properties of $\mathbf{z}_{pk}^H\hat{\mathbf{M}}_{\mathrm{PFP}}^{-1}\mathbf{z}_{pk}$ are independent of $\mathbf{M}$.

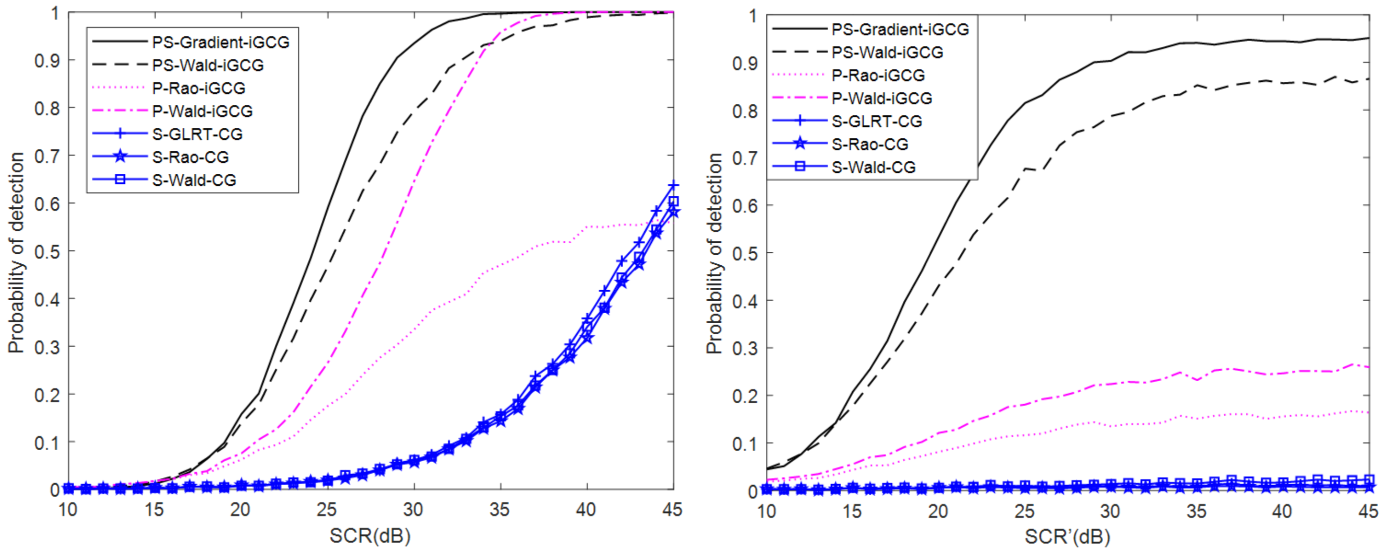

(a) $\cos^2\varphi=1$ (b) $\cos^2\varphi=0.5$

Figure 14. P_d vs. SCR for $N=8, K=5, R=8, r=3, \rho=0.9, h0=3, q=3, \beta=4, cos^2\phi=0.5,1$.

Then, define the unitary matrix $\mathbf{E}$ as

$$\mathbf{E}=\left[\mathbf{E}_{\overline{U}}, \mathbf{E}_2\right] \tag{A.3}$$

where $\mathbf{E}_{\overline{U}}=\overline{\mathbf{U}}\left(\overline{\mathbf{U}}^H\overline{\mathbf{U}}\right)^{-1/2}$, $\mathbf{E}_2^H\mathbf{E}_{\overline{U}}=\mathbf{0}_{(N-r)\times r}$ and $\mathbf{E}_2^H\mathbf{E}_2=\mathbf{I}_{N-r}$.

Let

$$\begin{cases}\overline{\mathbf{z}}_{\overline{U},pk}=\mathbf{E}_{\overline{U}}^H\overline{\mathbf{z}}_{pk}\\ \overline{\mathbf{z}}_{2,pk}=\mathbf{E}_2^H\overline{\mathbf{z}}_{pk}\end{cases} \tag{A.4}$$

Then we have

$$\overline{\mathbf{z}}_{pk}^H\overline{P}\overline{\mathbf{z}}_{pk}=\overline{\mathbf{z}}_{2,pk}^H\mathbf{E}_2^H\overline{\mathbf{P}}\mathbf{E}_2\overline{\mathbf{z}}_{2,pk} \tag{A.5}$$

Next, we partition the matrix $\mathbf{E}^H\overline{\mathbf{M}}\mathbf{E}$ as

$$\mathbf{E}^H\overline{\mathbf{M}}\mathbf{E}=\begin{bmatrix}\mathbf{M}_{11} & \mathbf{M}_{12}\\ \mathbf{M}_{21} & \mathbf{M}_{22}\end{bmatrix} \tag{A.6}$$

Based on the matrix inversion lemma [48], coupled with some additional computations, we can derive

$$\mathbf{E}_2^H\overline{\mathbf{P}}\mathbf{E}_2=\overline{\mathbf{M}}_{22}^{-1} \tag{A.7}$$

Substitute (A.7) into (A.5), and we obtain

$$\overline{\mathbf{z}}_{pk}^H\overline{\mathbf{P}}\overline{\mathbf{z}}_{pk}=\overline{\mathbf{z}}_{2,pk}^H\overline{\mathbf{M}}_{22}^{-1}\overline{\mathbf{z}}_{2,pk} \tag{A.8}$$

Obviously, after unitary transformation (A.4) and (A.6), $\overline{\mathbf{z}}_{2,pk}$ and $\overline{\mathbf{M}}_{22}$ follow the distributions respectively of.

$$\begin{cases}\overline{\mathbf{z}}_{2,pk}\sim\mathbf{CN}\left(\mathbf{0}_{(N-r)\times 2},\mathbf{I}_{N-r}\right)\\ \overline{\mathbf{M}}_{22}\sim\mathbf{CW}\left(2R,\mathbf{I}_{N-r}\right)\end{cases} \tag{A.9}$$

Thus, the asymptotic statistical properties of $\overline{\mathbf{z}}_{pk}^H\overline{\mathbf{P}}\overline{\mathbf{z}}_{pk}$ in (A.8) are not influenced by $\mathbf{M}$ under H_0.

In summary, both the PS-Gradient-iGCG (or equivalent PS-Rao-iGCG) and PS-Wald-iGCG exhibit asymptotic CFAR properties w.r.t the structure of the unknown CCM.

Data Availability Statement

Data will be made available on request.

Funding

This work was supported in part by the National Natural Science Foundation of China under Grant 62471483 and Grant 61971432; in part by the Taishan Scholar Project of Shandong Province under Grant tsqn201909156.

Conflicts of Interest

Xiaoming Tang is an employee of The 3H Company, Yantai 264001, China.

Ethical Approval and Consent to Participate

Not applicable.

References

[1] Liu, W., Liu, J., Hao, C., Gao, Y., & Wang, Y. (2022). Multichannel adaptive signal detection: Basic theory and literature review. *Science China Information Sciences, 65*(2), 121301. [CrossRef]

[2] Jian, T., He, J., Liu, Y., He, Y., Xu, C., & Xie, Z. (2023). Persymmetric adaptive detection of range-spread targets in subspace interference plus Gaussian clutter. *Science China Information Sciences, 66*(5), 152306. [CrossRef]

[3] Tang, P., Dong, R., Liu, W., & Liu, J. (2022). Adaptive multichannel detectors for distributed target based on Gradient test. *Signal Processing, 191*, 108350. [CrossRef]

[4] Ciuonzo, D., De Maio, A., & Orlando, D. (2016). A unifying framework for adaptive radar detection in homogeneous plus structured interference—Part I: On the maximal invariant statistic. *IEEE Transactions on Signal Processing, 64*(11), 2894–2906. [CrossRef]

[5] Ciuonzo, D., De Maio, A., & Orlando, D. (2016). A unifying framework for adaptive radar detection in homogeneous plus structured interference—Part II: Detectors design. *IEEE Transactions on Signal Processing, 64*(11), 2907–2919. [CrossRef]

[6] Liu, W., Xie, W., Liu, J., & Wang, Y. (2014). Adaptive double subspace signal detection in Gaussian background—Part I: Homogeneous environments. *IEEE Transactions on Signal Processing, 62*(9), 2345–2357. [CrossRef]

[7] Ren, Z., Yi, W., Kong, L., & Yang, X. (2023). Adaptive range and doppler distributed target detection in non-Gaussian clutter. *IEEE Transactions on Signal Processing, 71*, 2376–2390. [CrossRef]

[8] Liu, W., Wu, Y., Jiang, Q., & Liu, J. (2025). Eigenvalue-based distributed target detection in compound-Gaussian clutter. *Science China Information Sciences*. [CrossRef]

[9] Shang, X., & Song, H. (2011). Radar detection based on compound-Gaussian model with inverse gamma texture. *IET Radar, Sonar & Navigation, 5*(3), 315–321. [CrossRef]

[10] Shang, X., Song, H., Wang, Y., & He, X. (2012). Adaptive detection of distributed targets in compound-Gaussian clutter with inverse gamma texture. *Digital Signal Processing, 22*(6), 1024–1030. [CrossRef]

[11] Cui, G., Kong, L., Yang, X., & Yang, J. (2012). The Rao and Wald tests designed for distributed targets with polarization MIMO radar in compound-Gaussian clutter. *Circuits, Systems, and Signal Processing, 31*(1), 237-254. [CrossRef]

[12] Chen, S., Kong, L., & Yang, J. (2013). Adaptive detection in compound-Gaussian clutter with inverse Gaussian texture. *Progress In Electromagnetics Research M, 28*, 157–167. [CrossRef]

[13] Li, N., Cui, G., Kong, L., & Yang, X. (2014). MIMO radar moving target detection against compound-Gaussian clutter. *Circuits, Systems, and Signal Processing, 33*(6), 1819-1839. [CrossRef]

[14] Mennad, A., Younsi, A., El Korso, M. N., Hamadouche, M., & Breloy, A. (2017). Adaptive detection of range-spread target in compound-Gaussian clutter without secondary data. *Digital Signal Processing, 60*, 90–98. [CrossRef]

[15] Bandiera, F., Orlando, D., & Ricci, G. (2009). CFAR detection strategies for distributed targets under conic constraints. *IEEE Transactions on Signal Processing, 57*(9), 3305–3316. [CrossRef]

[16] Bandiera, F., De Maio, A., & Ricci, G. (2007). Adaptive CFAR radar detection with conic rejection. *IEEE Transactions on Signal Processing, 55*(6), 2533–2541. [CrossRef]

[17] Coluccia, A., & Ricci, G. (2018). A random-signal approach to robust radar detection. In *2018 52nd Annual Conference on Information Sciences and Systems* (*CISS*) (pp. 1–6). IEEE. [CrossRef]

[18] Liu, W., Liu, J., Gao, Y., Wang, G., & Wang, Y. L. (2020). Multichannel signal detection in interference and noise when signal mismatch happens. *Signal Processing, 166*, 107268. [CrossRef]

[19] Wang, Z., Liu, W., & Chen, H. (2024). *Adaptive detection for multichannel signals in non-ideal environments*. CRC Press.

[20] Sun, M., Liu, W., Liu, J., & Xie, W. (2024). Multiple subspace-based target detection in deterministic interference. *IEEE Signal Processing Letters, 31*, 3134–3138. [CrossRef]

[21] Bandiera, F., De Maio, A., Greco, A. S., & Ricci, G. (2007). Adaptive radar detection of distributed targets in homogeneous and partially homogeneous noise plus subspace interference. *IEEE Transactions on Signal Processing, 55*(4), 1223–1237. [CrossRef]

[22] Liu, W., Liu, J., Huang, L., Wang, Y., & Wang, Y. (2015). Rao tests for distributed target detection in interference and noise. *Signal Processing, 117*, 333–342. [CrossRef]

[23] Liu, W., Liu, J., Li, H., & Wang, Y. (2019). Multichannel signal detection based on Wald test in subspace interference and Gaussian noise. *IEEE Transactions on Aerospace and Electronic Systems, 55*(3), 1370–1381. [CrossRef]

[24] Jiang, Q., Wu, Y., Liu, W., & Liu, J. (2023). Subspace-based distributed target detection in compound-Gaussian clutter. *Digital Signal Processing, 140*, 104141. [CrossRef]

[25] Balleri, A., Nehorai, A., & Wang, J. (2007). Maximum likelihood estimation for compound-Gaussian clutter with inverse gamma texture. *IEEE Transactions on Aerospace and Electronic Systems, 43*(2), 775–779. [CrossRef]

[26] Gao, Y., Ji, H., & Liu, W. (2019). Persymmetric adaptive subspace detectors for range-spread targets. *Digital Signal Processing, 89*, 116–123. [CrossRef]

[27] Liu, J., Jian, T., Liu, W., & Wang, Y. (2020). Persymmetric adaptive detection with improved robustness to steering vector mismatches. *Signal Processing, 176*, 107669. [CrossRef]

[28] Aubry, A., De Maio, A., Foglia, G., & Orlando, D. (2015). Diffuse multipath exploitation for adaptive radar detection. *IEEE Transactions on Signal Processing, 63*(5), 1268–1281. [CrossRef]

[29] Zhang, J., Wang, Z., Zhao, Z., & He, Q. (2020). Persymmetric adaptive detection with reduced-dimension approach. *IEEE Signal Processing Letters, 27*, 565–569. [CrossRef]

[30] Jian, T., Wang, Z., & Wang, H. (2022). Ship target HRRP meta-learning recognition with small samples based on loss weighted correction. *Journal of Signal Processing, 38*(12), 2460–2468.

[31] Liao, X., Xie, J., & Zhou, J. (2023). Compound-Gaussian Spatial-Temporal Correlated Complex Clutter Simulation Based on a Two-Step Data-Driven Method. *IEEE Transactions on Aerospace and Electronic Systems, 59*(6), 9512-9526. [CrossRef]

[32] Huang, P., Yang, H., Zou, Z., Xia, X. G., & Liao, G. (2022). Multichannel clutter modeling, analysis, and suppression for missile-borne radar systems. *IEEE Transactions on Aerospace and Electronic Systems, 58*(4), 3236-3260. [CrossRef]

[33] Shi, X., Yang, C., Wang, X., & He, Y. (2023). Dual-Polarimetric persymmetric adaptive subspace detector for range-spread targets in heavy-tailed non-Gaussian clutter. *IEEE Geoscience and Remote Sensing Letters, 20*, 1–5. [CrossRef]

[34] Hao, C., Gazor, S., Foglia, G., & Maio, A. D. (2015). Persymmetric adaptive detection and range estimation of a small target. *IEEE Transactions on Aerospace and Electronic Systems, 51*(4), 2590–2604. [CrossRef]

[35] Wang, Z., Li, M., Chen, H., & Liu, W. (2016). Persymmetric detectors of distributed targets in partially homogeneous disturbance. *Signal Processing, 128*, 382–388. [CrossRef]

[36] Gao, Y., Liao, G., Zhang, S., & Liu, W. (2013). A persymmetric GLRT for adaptive detection in compound-Gaussian clutter with random texture. *IEEE Signal Processing Letters, 20*(6), 615–618. [CrossRef]

[37] Guo, X., Tao, H., Zhao, H. Y., & Liu, Y. (2017). Persymmetric Rao and Wald tests for adaptive detection of distributed targets in compound-Gaussian noise. *IETF Radar, Sonar & Navigation, 11*(3), 453–458. [CrossRef]

[38] Xu, Z., Liu, W., Wu, C., Du, Q., & Liu, J. (2025). Statistical Performance of Generalized Direction Detectors with Known Spatial Steering Vector. *IEEE Signal Processing Letters*. [CrossRef]

[39] Liu, J., Liu, W., Hao, C., & Gao, Y. (2020). Persymmetric subspace detectors with multiple observations in homogeneous environments. *IEEE Transactions on Aerospace and Electronic Systems, 56*(4), 3276–3284. [CrossRef]

[40] Sun, M., Liu, W., Liu, J., & Xie, W. (2021). Adaptive subspace detection based on Gradient test for orthogonal interference. *IEEE Transactions on Aerospace and Electronic Systems, 58*(3), 1868–1877. [CrossRef]

[41] Sun, M., Liu, W., Liu, J., & Hao, C. (2021). Rao and Wald tests for target detection in coherent interference. *IEEE Transactions on Aerospace and Electronic Systems, 58*(3), 1906-1921. [CrossRef]

[42] Van Trees, H. L. (2002). *Optimum array processing: Part IV of detection, estimation, and modulation theory*. John Wiley & Sons. [CrossRef]

[43] Gini, F., & Greco, M. (2002). Covariance matrix estimation for CFAR detection in correlated heavy tailed clutter. *Signal Processing, 82*(12), 1847–1859. [CrossRef]

[44] Liu, J., Gao, Z., Sun, Z., & Wang, Y. (2022). Detection architecture with improved classification capabilities for covariance structures. *Digital Signal Processing, 123*, 103404. [CrossRef]

[45] Conte, E., De Maio, A., & Ricci, G. (2001). GLRT-based adaptive detection algorithms for range-spread targets. *IEEE Transactions on Signal Processing, 49*(7), 1336–1348. [CrossRef]

[46] Wang, Z., Zhao, Z., Ren, C., & He, Q. (2019). Adaptive GLR-, Rao- and Wald-based CFAR detectors for a subspace signal embedded in structured Gaussian interference. *Digital Signal Processing, 92*, 139–150. [CrossRef]

[47] McMaster IPIX radar. (2001). Cognitive Systems Laboratory – McMaster University. (Accessed on 01 November 2025). Archived at: https://web.archive.org/web/20170712063506/https://soma.ece.mcmaster.ca/ipix/

[48] Harville, D. A. (1998). *Matrix algebra from a statistician's perspective*. Springer. [CrossRef]

Tao Jian was born in Hubei Province, P.R. China. He received the Ph.D. degrees in electronic engineering from Naval Aviation University, Yantai, P.R. China, in 2011, and has also been nominated for National Outstanding Doctoral Dissertation Award in 2013. He is currently a professor with Research Institute of Information Fusion, Naval Aviation University, Yantai, P.R. China, engaged in research on radar target adaptive detection. Dr. Jian has also served as a senior member of Chinese Institute of Electronics (CIE) and a committeeman of Signal Processing Branch in CIE. (Email: work_jt@163.com)

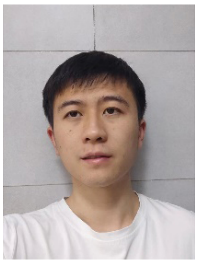

Zikeng Xie was born in Hunan Province, P.R. China, he received the B.S. and the M.S. degrees in Electronic Engineering from the Naval Aviation University, Yantai, China, in 2020 and 2022, respectively. (Email: 1397850644@qq.com)

Lei Guo was born in Jiangxi Province, P.R. China, he is an engineer and serves in Unit 92830 of the PLA. (Email: 149866577@qq.com)

Jia He was born in Hunan Province, P.R. China, he received the B.S. and the M.S. degrees in Electronic Engineering from the Naval Aviation University, Yantai, China, in 2020 and 2022, respectively. He is currently pursuing a Ph.D. degree and engaged in research on radar signal processing. (Email: 15653871521@163.com)

Xiaoming Tang was born in Zhejiang Province, P.R. China, he received the Ph.D. degree from Naval University of Engineering, in 2004. He is the CEO and associate professor of 3H company. His research interests include radar target detection and recognition. (Email: 757175330@qq.com)